Volume 1 | Number 1 | Jan 2013 | Pages 1–100

Journal of
Materials Chemistry A

Materials for energy and sustainability
www.rsc.org/materialsA

Li⁺

ROYAL SOCIETY
OF CHEMISTRY

ROYAL SOCIETY
OF **CHEMISTRY**

www.rsc.org/materialsA

ARTICLE TYPE

Facile synthesis and superior electrochemical performances of CoNi$_2$S$_4$/graphene nanocomposite suitable for supercapacitor electrodes

Weimin Du,*[a] Zhiyong Wang,[a] Zhaoqiang Zhu,[a,b] Sen Hu,[a] Xiaoyan Zhu,[a] Yunfeng Shi,[a] Huan Pang,*[a] and Xuefeng Qian[c]

A facile physic approach was developed to construct CoNi$_2$S$_4$/graphene nanocomposite. As-obtained samples are detailed characterized and evaluated the corresponding electrochemical performances. Results show the supercapacitor electrodes based on CoNi$_2$S$_4$/graphene nanocomposite exhibit excellent
10 pseudocapacitance behaviour enhanced by synergistic effect. When the loaded amount of graphene is 5% (wt.%), the maximum specific capacitance reaches up to 2009.1 F g^{-1} at a discharge current density of 1 A g^{-1} and the specific capacitance can be maintained as 755.4 F g^{-1} at 4 A g^{-1} after 2000 charge-discharge cycles. Meantime, this electrode shows excellent rate capability (1046.4 F g^{-1} at 20 A g^{-1}) and better electrochemical reversibility. This enhancement in pseudocapacitance behaviour is due to the
15 CoNi$_2$S$_4$/graphene interconnected conductive network which promotes not only electrolyte diffusion and efficient charge transport, but also prevents aggregation and volume expansion/contraction of electroactive materials. Hence one can see that CoNi$_2$S$_4$/graphene nanocomposite is a promising electrode material of high-performance supercapacitors.

Introduction

20 Various carbon nanomaterials have been selected as electrode materials of supercapacitors (SCs) due to the unique chemical and physical properties, *i.e.*: high conductivity, large surface-area, excellent corrosion resistance, thermal stability, and cost effectiveness, *etc*.[1, 2] However, lower specific capacitance of
25 single-phase carbon nanomaterials largely restricts the commercial application as electrode materials of SCs (*e.g.*: 125 F g^{-1} for porous carbon,[3] 327 F g^{-1} for hierarchical carbon [4] and 212 F g^{-1} for reduced graphene oxide paper,[5] *etc*). Therefore, the utility of carbon-based nanomaterials as substrates of transition
30 metal oxides or hydroxides in supercapacitors and Li-ion batteries has raised more and more interests in recent years.[6, 7] In such carbon-based composite electrodes, carbon nanomaterials not only serve as the physical support but also provide the channels for charge transport. Also, higher electronic conductivity of
35 carbon nanomaterials benefits to the rate capability and power density at a large charge/discharge current.[8, 9] Especially, two-dimensional (2-D) graphene (GR) is even easier and more flexible to integrate with metal compounds compared with zero-dimensional (0-D) carbon nanoparticles and one-dimensional (1-
40 D) carbon nanowires. Thus, GR has been used as the ideal matrix for prevent the electroactive nanomaterials from agglomeration and separate from the surface of graphene sheets to improve electrochemical activity. The notable synergistic effect between the graphene layers and electroactive nanomaterials can provide a
45 large surface area to improve the diffusion rate of ions, leading to

higher specific capacitance and rate capability. Therefore, GR-based electrode materials of SCs have been devoted many efforts and the researches about graphene/metal oxide composite electrodes have been reviewed in the recent articles.[10, 11]

50 As the potential electrode materials of SCs, ternary cobalt nickel oxides (*e.g.*: Ni$_x$Co$_{3-x}$O$_4$) possess some obvious advantages, *e.g.*: richer redox chemistry, higher electrochemical activity, low-cost and at least two orders of magnitude higher electronic conductivity than simple oxides. However, compared to
55 significant advances of the cobalt (or nickel) oxides, hydroxides, and sulfides,[12-18] the studies about ternary cobalt nickel oxides have been lagged a lot. Lately, some single-phase materials or composite of Ni$_x$Co$_{3-x}$O$_4$ have been synthesized and excellent electrochemical energy storage properties were obtained, *e.g.*:
60 nanosheets,[19, 20] nanoneedle,[21] nanowires,[22] and microbelts,[23] of NiCo$_2$O$_4$; Ni$_{0.3}$Co$_{2.7}$O$_4$ hierarchical structures;[24] NiCo$_2$O$_4$/carbon nanotubes (CNT)[25] and NiCo$_2$O$_4$/graphene oxide (GO),[26] *etc*. It should be specially noted that the NiCo$_2$O$_4$ nanosheets reported by Lou *et al* exhibited excellent rate capability. The specific
65 capacitance can reach up to 1450 F g^{-1} even at a higher current density of 20 A g^{-1}.[19] Similar to ternary cobalt nickel oxides, ternary cobalt nickel sulfides (CoNi$_2$S$_4$ or NiCo$_2$S$_4$) are also expected to offer richer redox reactions than the single component sulfides due to the contributions from nickel and
70 cobalt ions. Furthermore, ternary cobalt nickel sulfides have higher electronic conductivity than Ni$_x$Co$_{3-x}$O$_4$.[27] Higher electrical conductivity can decrease both the sheet resistance and the charge transfer resistance of the electrode which causes a

smaller interior resistance (IR) loss at a higher current density. As a result, higher rate capability and power density can be achieved.[11] Thus, ternary cobalt nickel sulfide nanostructures are another outstanding electrode material of supercapacitors. More
5 recently, two works about single-phase $NiCo_2S_4$ were explored, *i. e.*: $NiCo_2S_4$ porous nanotubes synthesis via sacrificial templates showing a specific capacitance of 933 F g^{-1} at 1 A g^{-1},[28] urchin-like $NiCo_2S_4$ obtained by a precursor transformation method with a high value of 1050 F g^{-1} at 2 A g^{-1}.[27] Nevertheless, the need for
10 premade templates or two-step transformation increases the cost of production. Hence, composite of $NiCo_2S_4$ nanosheets/graphene was further fabricated by a hydrothermal method with higher specific capacitance of 760 F g^{-1} at 20 A g^{-1}.[29] However, to the best of our knowledge, less report is available about the synthesis
15 and supercapacitive properties of $CoNi_2S_4$ nanomaterials and $CoNi_2S_4$/graphene nanocomposite. Thus, a one-step solvothermal process was successfully developed to synthesize $CoNi_2S_4$ nanoparticles in a just-published communication from our research team. [30] When applied as electrode materials of SCs,
20 $CoNi_2S_4$ nanoparticles with lower cost of production exhibited higher specific capacitance (1169 F g^{-1} at current densities of 1 A g^{-1}). But the rate capability was not good enough. In order to further expand the commercial application of $CoNi_2S_4$ nanoparticles for high-performance supercapacitors, the present
25 work provides a simple physic approach to fabricate $CoNi_2S_4$/graphene nanocomposite. The as-obtained samples were detailed characterized and investigated the electrochemical performances. Results show that the electrode based on $CoNi_2S_4$/graphene nanocomposite exhibit superior
30 electrochemical performances enhanced by synergistic effect when the loaded amount of graphene is 5% (wt.%), *i.e.*: higher specific capacitance, good cycling stability, excellent rate capability, and better electrochemical reversibility. It suggests the great potential of $CoNi_2S_4$/graphene nanocomposite in high-
35 performance supercapacitor electrodes.

Experimental

Synthesis of CoNi₂S₄/graphene nanocomposite

Typical $CoNi_2S_4$ (*abbr.* CNS) nanoparticles were synthesized according to our just-published work.[30] The Graphene (GR) was
40 prepared from natural graphite by a modified Hummers method.[31] Detailed synthetic process was provided in Electronic Supplementary Information (ESI†). $CoNi_2S_4$/graphene nanocomposite was obtained by a simple physic process. According to a certain weight ratio (wt.%) of synthesized GR
45 (GR : CNS = 5 : 100), as-synthesized CNS nanoparticles and GR sheets were mixed in 20 mL absolute ethanol at room temperature. The mixture was ultrasonic for 30 minute until there is not obvious particulate matter. After magnetically stirred for 24 hours, the turbid liquid was centrifuged and dried in a vacuum oven.
50 Finally, $CoNi_2S_4$/graphene nanocomposite with 5% loaded amount of GR was obtained and labelled as CNS@5%GR. As a contrast, $CoNi_2S_4$/graphene nanocomposite with different loaded amount of GR (*e.g.*: 1%, 3%, 10%, 30%) were also synthesized by the similar process and labelled as CNS@1%GR,
55 CNS@3%GR, CNS@10%GR and CNS@30%GR.

Structural characterizations

Crystal structures of the products were characterized on a Rigaku Ultima III X-ray diffractometer (XRD) equipped with a Cu *Kα* radiation source (λ=0.15418 nm). The chemical state of products
60 was analyzed using X-ray Photoelectron Spectroscopy (XPS, PHI 5000 VersaProbe). Surface morphologies of samples were studied by Scanning Electron Microscope (SEM, Japan, JSM 6701). FTIR spectra were recorded on a Perkin Elmer Paragon 1000 FT-IR Spectrometer. Optical properties were determined by
65 measuring solid UV-Vis spectra using UV-Vis spectrophotometer (Shimadzu, Uv-2550). The surface area of the product was calculated from N_2 adsorption/desorption isotherms at 77 K that were conducted on a Gemini VII 2390 Analyzer. Prior to measurement, all samples were outgassed at 110 ^{o}C for 120
70 minutes under flowing N_2.

Electrochemical measurements

Working electrodes were prepared by mixing as-synthesized active material (85 wt%) with acetylene black (10 wt%) and poly(tetrafluoroethylene) (5 wt%), coating on a piece of foamed
75 nickel of about 1 cm^2 and pressing to be a thin foil at a pressure of 10 MPa. The weight of active material is about 5 mg. All electrochemical properties of self-made single electrode, including cyclic voltammetry (CV), galvanostatic charge–discharge (CD), electrochemical impedance spectrometry (EIS),
80 and cycle stability, were carried out at room temperature in a three-electrode system equipped with platinum electrode and a saturated calomel electrode (SCE) as counter and reference electrodes, respectively. The electrolyte was 3.0 M KOH solution. CV and CD tests were measured by an electrochemical
85 working station (CHI660E, Chenghua, Shanghai, China). Cycle stability tests were carried out with an Arbin electrochemical instrument. EIS measurements of all the samples were conducted at open-circuit voltage in the frequency range of 100 kHz to 0.01 Hz with AC voltage amplitude of 5 mV using PARSTAT2273
90 advanced electrochemical system.

Results and Discussion

Structural characterizations and chemical state of typical CoNi₂S₄ sample

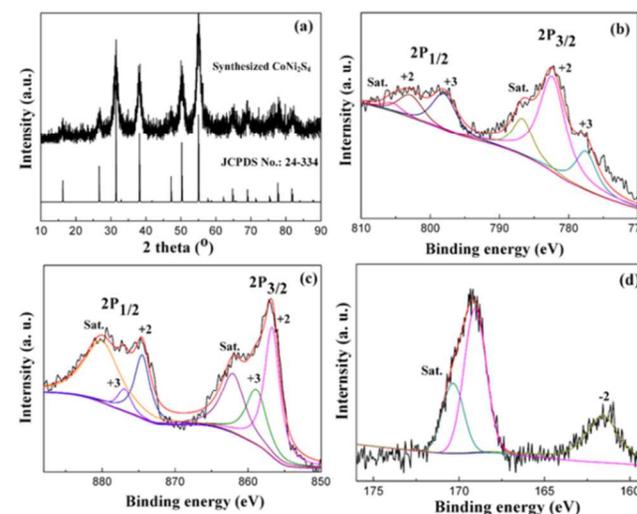95 **Fig. 1** (a) XRD pattern and (b-d) XPS spectra of Co 2p, Ni 2p, and S 2p; of the typical $CoNi_2S_4$ sample

X-ray diffraction (XRD) patterns of the standard data and typical $CoNi_2S_4$ sample are shown in Fig. 1a. All of the diffraction peaks of typical sample can be indexed to the cubic phase of $CoNi_2S_4$ (JCPDS No.: 24-334) with the *Fd-3m* space group and a primitive
5 cubic unit cell $a = 9.4279$ Å. No peaks from other phases were detected, *e.g.*: CoS, NiS, oxides or organic compounds related to the reactants indicating that the product is of high purity. For confirming the chemical state in $CoNi_2S_4$, X-ray photoelectron spectroscopy (XPS) measurements were conducted and the
10 results are presented in Fig. 1b-1d. By using a Gaussian fitting method, the *Co* 2p spectrum (Fig. 1b) can be best fitted with two spin-orbit doublets and two shake-up satellites (identified as "Sat."). One pair is corresponds to *Co* 2P 3/2 and *Co* 2P 1/2 centered at 777.7 eV and 798.2 eV, respectively.[32] Another pair
15 binding energies for were appeared in higher energy region about 782.5 eV and 803.0 eV. These two pairs of doublet peaks of *Co* 2P indicate that there exist two kinds of cobalt oxidation state: *i. e.*: Co^{2+} and Co^{3+}. Similarly, the *Ni* 2p spectrum (Fig. 1c) can also be best fitted by considering two spin-orbit doublets characteristic
20 of Ni^{2+} and Ni^{3+} and two shake-up satellites. These results match well with the reported data in $NiCo_2O_4$ [22, 33] and $NiCo_2S_4$.[27] The *S* 2P spectrum can be divided into two main peaks and one shake-up satellite. The binding energy at 161.6 eV is typical of metal–sulphur bonds in the ternary metal sulfides.[34] The binding energy
25 at 169.0 eV can be attributed to the sulphur ion with higher oxide state of $S_4O_6^{2-}$ at the surface[35, 36] which can be ascribed to partly oxidation of $CoNi_2S_4$. According to the XPS analysis, the near-surface of the $CoNi_2S_4$ has a composition of Co^{2+}, Co^{3+}, Ni^{2+}, Ni^{3+} and S^{2-}, $S^{2.5+}$. Based on the TEM observations in our
30 previous work,[30] the as-prepared $CoNi_2S_4$ (CNS) was consisted of single-crystalline nanoparticles with the size of 8-15 nm.

Structural and morphological characterizations of GR and $CoNi_2S_4$/graphene nanocomposite
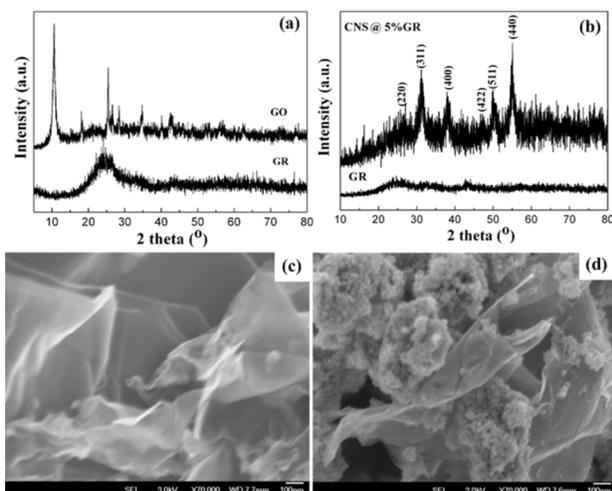

35 **Fig. 2** XRD patterns of (a) graphene oxide (GO) and graphene (GR), (b) GR and $CoNi_2S_4$/graphene nanocomposite with 5% loaded amount of GR (CNS@5%GR); SEM images of (c) GR and (d) CNS@5%GR nanocomposite

Commercial graphite is usually higher crystalline and the XRD
40 diffraction intensity is much higher than those of GO and GR (See ESI† Fig. S1). So, the obvious decrease of the diffraction intensity of GO and GR implied the layered structure of

commercial graphite is greatly damaged. The amplified XRD patterns of the GO and the GR samples are shown in Fig. 2a. In
45 the XRD pattern of the GO, the typical sharp peak around 10° can be detected, which corresponding to the (002) plane of GO.[5] After reduction, the GO peak disappeared and a broadened peak at 24.5° emerged. This indicates that the higher degree of the deoxygenation of GO and GO was reduced to GR. It can be seen
50 from Fig. 2b that the XRD pattern of CNS@5%GR is similar to that of free CNS nanoparticles. Five characteristic peaks at 26.68°, 31.53°, 38.18°, 50.12°, and 55.04° correspond to the (220), (311), (400), (511), and (440) diffraction planes, respectively. It is noteworthy that the diffraction peaks of *C* from GR could not be
55 observed in the XRD pattern of the CNS@5%GR nanocomposite, which is mainly due to the lower diffraction intensity of GR. Other $CoNi_2S_4$/graphene nanocomposites with different loaded amount of GR (CNS@1%GR, CNS@3%GR, CNS@10%GR and CNS@30%GR) have the similar XRD patterns. Super-thin
60 graphite sheets shown in SEM image (Fig. 2c) clearly indicate the successful preparation of GR nanosheets. Also, it can be found in Fig. 2d that there are both CNS nanoparticles and GR nasnosheets in CNS@5%GR nanocomposite demonstrating the formation of $CoNi_2S_4$/graphene nanocomposite. From the FTIR
65 pattern of GR and CNS@5%GR shown in ESI† Fig. S2, the typical skeletal vibration of *C=C* in pure graphene nanosheets appeared at 1625 cm^{-1}, confirming the formation of SP^2 carbon skeleton. But in CNS@5%GR nanocomposite, the skeletal vibration of *C=C* shifted to the higher wavenumber of 1633 cm^{-1}.
70 The vibration-peak shift implies the interaction between GR nanosheets and CNS nanoparticles and the formation of $CoNi_2S_4$/graphene nanocomposite.

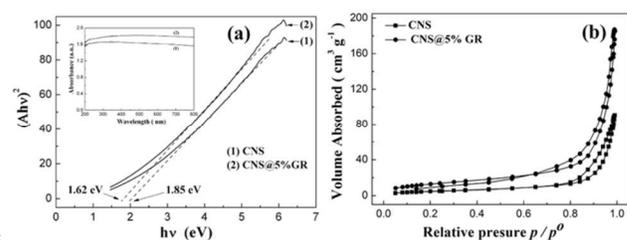**Microstructure analysis of CNS nanoparticles and CNS@5%GR nanocomposite**

75 **Fig. 3** (a) $(Ahv)^2$ –hv curves and UV–vis adsorption spectra (the inset), (b) Nitrogen adsorption–desorption isotherms of CNS nanoparticles and CNS@5%GR nanocomposite

To evaluate the band gap, the UV–vis absorption spectrum is
80 measured (Fig 3a). CNS nanoparticles and CNS@5%GR nanocomposite have better light absorption in the visible range (400 ~ 800nm) which is consistent with the black appearance. Generally, the band gap energy, E_g, can be determined by the following equation: $(Ahv)^n = K(hv – E_g)$, where hv is the
85 photoenergy, *A* is the absorbance, *K* is a constant relative to the material, and *n* is either 2 for a direct transition or 1/2 for an indirect transition. $CoNi_2S_4$ is semiconducting with direct transition and $n = 2$. [27] Hence, the band gap energies of CNS and CNS@5% GR nanocomposite are calculated to be about 1.85 eV
90 and 1.62eV, respectively. The decrease of the band-gap energy of CNS@5%GR nanocomposite can be ascribed to the higher conductivity of GR. Moreover, both of them show much lower

Eg than NiCo$_2$O$_4$, i.e.: 2.4 and 3.6 eV which is beneficial for the fast transfer of the electron. Fig. 3b shows the nitrogen adsorption–desorption isotherms. It is worth noting that the surface area of CNS@5%GR nanocomposite (48.4 m^2·g^{-1}) was higher than that of CNS nanoparticles (18.64 m^2·g^{-1}). This feature is due to the contribution of GR to surface area and/or the presence of the CNS nanoparticles adhered on GR sheets that created enhanced surface-area-contributing voids between adjacent nanoparticles. The overall surface area of the CNS@5%GR nanocomposite was smaller than the reported research of NiCo$_2$O$_4$/graphene oxide nanocomposite.[26] But according to a previous review, the specific capacitance of various materials does not linearly increase with the specific surface area.[37] In a word, GR plays an important role on increasing the conductivity and surface area of CoNi$_2$S$_4$ nanoparticles.

Electrochemical performance of CoNi$_2$S$_4$/graphene nanocomposite, CNS nanoparticles, and GR
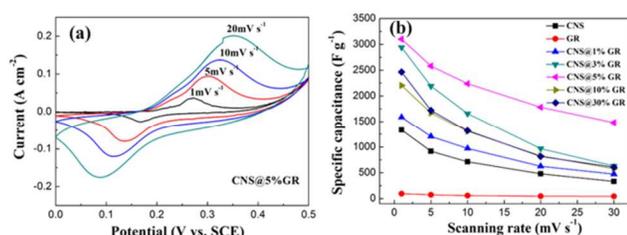

Fig. 4 (a) CV curves at different scanning rates recorded from supercapacitor electrodes consisting of CNS@5%GR nanocomposite; (b) specific capacitances comparison chart between CoNi$_2$S$_4$/graphene nanocomposite, CNS nanoparticles, and GR at different scanning rates

Electrochemical properties of the supercapacitor electrodes based on CoNi$_2$S$_4$/graphene nanocomposite, CNS nanoparticles, and GR are investigated by means of CV tests and CD in a three-electrode cell with 3 M KOH aqueous solution as electrolyte. Fig. 4a shows CV curves of the CNS@5%GR nanocomposite electrode at various scan rates ranging from 1 to 20 mV s^{-1}. Apparently, the CV curves of the CNS@5%GR nanocomposite electrode suggest two pairs of well-defined redox peaks within 0–0.5 V (vs. SCE). These peaks mainly originate from Faradaic redox reactions related to Co^{2+}/Co^{3+} and Ni^{2+}/Ni^{3+} redox couples, and probably mediated by the OH$^-$ ions in the alkaline electrolyte.[29] This typical pseudocapacitive characteristic of CNS@5%GR nanocomposite is obviously distinct from the electric double-layer capacitance characterized by nearly rectangular CV curves. The reduction peak current and the oxidation peak current were constrained between -0.25A cm^{-2} and +0.25A cm^{-2}. Compared with the CV curves of CNS nanoparticles (ESI† Fig. S3a), the CV curve of CNS@5%GR nanocomposite showed a larger encircled area, suggesting the higher capacitance. The CV curve of GR-based electrode materials presented a quasi-rectangular shape which is consistent with the feature of electrostatic double-layer capacitors (ESI† Fig. S3b). As for CoNi$_2$S$_4$/graphene nanocomposite with different loaded amount of GR (*e.g.*: 1%, 3%, 10%, 30%), the shapes of CV curves are similar with those of CNS@5%GR nanocomposite (See ESI† Fig. S4). In order to obtain a better visualization of the influence of GR on the peak current signals of CoNi$_2$S$_4$/graphene nanocomposite, the CV curves at 10 mV S^{-1} recorded from supercapacitor electrodes

consisting of CoNi$_2$S$_4$/graphene nanocomposite with different loaded amount of GR were provided in ESI† Fig. S5. It can be seen that the CNS@5%GR nanocomposite showed focused peak current signal and symmetric redox peaks implying the best match between CNS nanoparticles and GR nanosheets.

The specific capacitance (Csp) of single electrode was calculated from the CV curve based on the following equation: [38]

$$C_{sp} = \frac{1}{mv(V_c - V_a)} \int_{Va}^{Vc} I(V)dV$$

where C_{sp} (F g^{-1}), m (g), v(V s^{-1}), Vc and Va, and I (A) are the specific capacitance, the mass of the active materials in the electrode, potential scan rate, high and low potential limits of the CV tests, and the instant current on CV curves, respectively. The average C_{sp} of CoNi$_2$S$_4$/graphene nanocomposite, CNS nanoparticles, and GR at different scanning rates was calculated and provided in Fig 4b. It is worth noting that CNS@5%GR nanocomposite has the highest Csp and the maximum value as high as 3102.6 F g^{-1} is obtained at a scan rate of 1 mV s^{-1} and a Csp value of 1782.8 F g^{-1} is obtained even at a high scan rate of 20 mV s^{-1}. These results indicate that CNS@5%GR nanocomposite has excellent power characteristics and are a promising material for supercapacitor applications. Meanwhile, single-phase CNS nanoparticles, CNS@1%GR，CNS@3%GR，CNS@10%GR and CNS@30%GR nanocomposite show an obvious decrease of Csp value and GR have the lowest specific capacitance with scanning rate increasing from 1 to 20 mV s^{-1}. Compared with the negligible C_{sp} from the GR (< 100F g^{-1}), one can safely confirm that the pseudocapacitance of CNS@5%GR nanocomposite mainly comes from the CNS nanoparticles rather than GR.
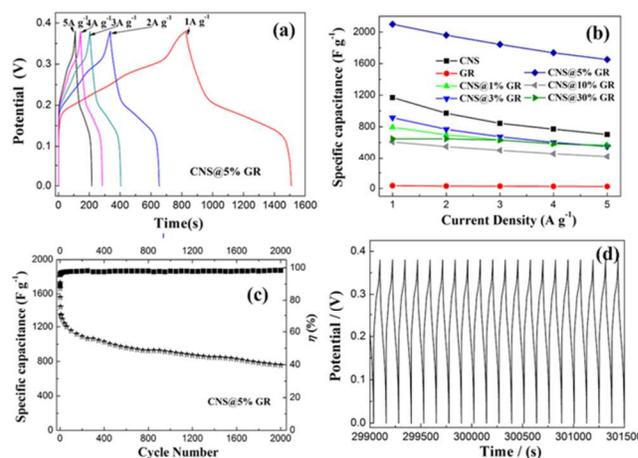

Fig. 5 (a) CD curves of supercapacitor electrodes based on CNS@5%GR nanocomposite; (b) specific capacitances comparison chart between CoNi$_2$S$_4$/graphene nanocomposite, CNS nanoparticles, and GR at different current densities; (c) Cycle performance and (d) the typical charge-discharge curves for the last 20 cycles at a current density of 4 A g^{-1} of CNS@5%GR nanocomposite

To further evaluate the application potential of the CoNi$_2$S$_4$/graphene nanocomposite as an electrode of SCs, CD measurements were carried out between 0 and 0.4 V (vs. SCE) at

various current densities ranging from 1 to 5 A g^{-1}, as shown in Fig. 5. As can be seen from the constant current charge-discharge curves of CNS@5%GR nanocomposite, the shape of five curves are very similar and show ideal capacitive behaviour with sharp responses and small internal resistance (IR) drop. In addition, there is a potential platform of in every discharge curve. [39] This indicates typical pseudocapacitance behaviour, caused by a charge transfer reaction or electrochemical absorption/desorption process at the electrode/electrolyte interface, which is in agreement with the result obtained from CV curves in Fig 4a. As for GR, all of the charging/discharging curves were fairly linear, again demonstrating electrostatic double-layer capacitive behaviour and the specific capacitance gradually decreased with the increase of discharge current density (See ESI† Fig. S6a). Compared with the CD curves of CNS nanoparticles (ESI† Fig. S6b), there are also some features of the CD curves of GR in those of CoNi$_2$S$_4$/graphene nanocomposite with different loaded amount of GR (*e.g.*: 1%, 3%, 5%, 10%, 30%) (See Fig. 5a and ESI† Fig. S7). The specific capacitances of all of the electrodes can be calculated based on the charge–discharge curves and the equation: $Csp = I \times \Delta t / (\Delta V \times m)$, where Csp (F g^{-1}) is the specific capacitance, I (A) is the discharge current, Δt (s) represents the discharge time, ΔV (V) is the potential change during discharge, and m (g) is the mass of the active material. It can be found in Fig. 5b that the specific capacitances of all of the electrodes decreased along with the increase of current density. This reduction of capacitance at high current density can be attributed to the low diffusion of the electrolyte ion. The ionic motion in the electrolyte is always limited by diffusion because of the time constraint during the high-rate charge–discharge process, and only the outer active surface is utilized for charge storage. [27] It also can be found from Fig. 5b that CNS@5%GR nanocomposite electrode exhibited excellent pseudocapacitances of 2099.1, 1961.6, 1843.7, 1737.5 and 1651.7 F g^{-1} at current densities of 1, 2, 3, 4 and 5 A g^{-1}. Therefore, CNS@5%GR nanocomposite possessed higher specific capacitances than CNS nanoparticles and GR. A synergistic effect obviously exists in the present CoNi$_2$S$_4$/graphene nanocomposite which also appeared in some previous works. [40-42] In CNS@5%GR nanocomposite electrodes, GR not only serve as the physical support of ternary metal sulfide but also provide the channels for charge transport. The electro-activities of ternary metal sulfides contribute to higher specific capacitance and higher energy density of the composite electrodes. When the load amount of GR is lower (*i.e.*:1%, 3%), CNS nanoparticles cannot well coat and channels for charge transport can not uniformly dispersed. When the load amount of GR is higher (*i.e.*:10%, 30%), the decrease of electro-activities CNS nanoparticles leads to the decrease of specific capacitance. Hence, the most suitable loaded amount of GR is 5% (wt.%) and CNS@1%GR, CNS@3%GR, CNS@10%GR and CNS@30%GR nanocomposite shows an obvious attenuation of Csp value.

Because long cycling life is an important requirement of supercapacitor applications, a cycling-life test was carried out for CNS@5%GR nanocomposite electrode by repeating the CD test between 0 and 0.4 V at the current density of 4 A g^{-1} for 2000 cycles. Although graphene could prevent the aggregation and volume expansion/contraction of electroactive materials, partial aggregation of CoNi$_2$S$_4$ nanoparticles can still take place.

Therefore, the Csp of CNS@5%GR nanocomposite electrode is decreased along with the increase of cycle number. However, due to the higher initial specific capacitance, a higher Csp of 755.4 F g^{-1} can still be kept after 2000 charge-discharge cycles (See Fig. 5c). As for single-phase CNS nanoparticle electrode, the Csp of only 377.7 F g^{-1} was remained after 2000 cycles. [30] Based on the SEM images of the film morphology of CNS@5% nanocomposite and CNS nanoparticles on the foamed nickel surface (See ESI† Fig. S8), it can be found that GR nanosheets indeed existed in the CNS@5%GR nanocomposite electrode. Therefore, this enhancement in cycling-life is due to the CNS@5%GR nanocomposite interconnected conductive network which promotes not only efficient charge transport and electrolyte diffusion, but also prevents the volume expansion/contraction and aggregation of electroactive materials. In addition, the charge-discharge efficiency (η), also called Coulombic efficiency, can be estimated according to following equation: $\eta = t_c / t_c \times 100\%$. where t_c and t_c are the charge and discharge intervals, respectively. CNS@5%GR nanocomposite electrode exhibited higher charge-discharge efficiency of $\sim$ 99% over the entire test. Typical charge-discharge curves for the last 20 cycles last at 4A g^{-1} are shown in Fig. 5d. It is found that the shapes of the CD curves were almost unchanged indicating better electrode reversibility of CNS@5%GR nanocomposite.
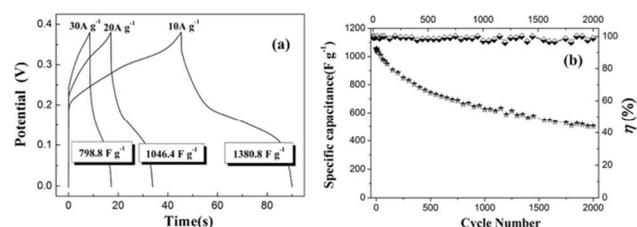

Fig. 6 (a) CD curves at 10, 20, 30A g^{-1}, (b) cycle life and Coulombic efficiency at 20A g^{-1} of CNS@5%GR nanocomposite.

Despite the significant advances achieved in supercapacitors, the high-rate capacitance is still insufficient. Higher specific capacitance cannot be well maintained under high rates including high scanning rate, high current density and high power operation, which are commonly found for most electroactive materials. Simultaneously increasing the rates of ion diffusion and electron transfer is an effective way to improve the rate capability of electrode materials. Therefore, CNS@5%GR nanocomposite with high conductivity might processes better high-rate electrochemical properties. It can be found in Fig. 6a, CNS@5%GR nanocomposite still kept higher Csp of 1380.8, 1046.4, 798.8 F g^{-1} even at higher current density of 10, 20, 30 A g^{-1}. Cycle life, Coulombic efficiency (Fig. 6b) and the charge–discharge curves for the last 20 cycles last at 20A g^{-1} (ESI† Fig. S9) again demonstrated that CNS@5%GR nanocomposite exhibit higher degree of reversibility after a long-term cycling test. Compared with the reported ternary cobalt nickel oxides/sulfides and single component sulfides with particle-like morphology, CNS@5%GR nanocomposite electrode exhibited higher specific capacitance and excellent rate capacity (See ESI† Table S1). Of course, there are two excellent electrochemical properties of foamed nickel supported nanosheet-like cobalt sulfide films[18] and NiCo$_2$O$_4$ nanosheets [19]. Their excellent performance were closely related with the foamed nickel supported nanosheet-like

nanostructures which can greatly increase the specific surface area, shorten the diffusion path of the OH⁻ ions, promote long-term stability and high rates. From here we can see that the morphologies have an important role on the electrochemical properties of electrode materials.
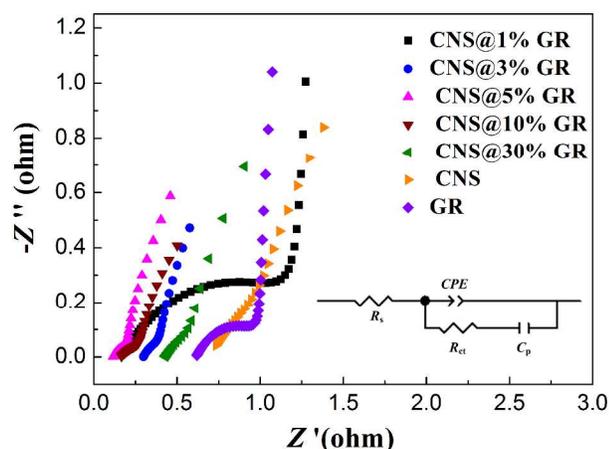

Fig. 7 Electrochemical impedance spectra for the supercapacitor electrodes based on CoNi$_2$S$_4$/graphene nanocomposite, CNS nanoparticles, and GR under room temperature in 3.0 M KOH solution; the insert is an equivalent circuit consisting of a bulk solution resistance R_s, a charge-transfer R_{ct}, a pseudocapacitive element C_P from redox process, and a constant phase element (CPE) to account for the double-layer capacitance

Electrochemical impedance spectroscopy (EIS) analysis is a principal method for examining the fundamental behaviour of electrode materials for supercapacitors. To further understand the electrical performance of CoNi$_2$S$_4$/graphene nanocomposite, we measured the impedance in the frequency range of 0.01–10^{5}Hz at open circuit potential with an AC perturbation of 5 mV. The Nyquist plot of the supercapacitor electrodes based on CoNi$_2$S$_4$/graphene nanocomposite, CNS nanoparticles, and GR was shown in Fig. 7. The values of C_p, R_{ct}, and CPE were calculated by ZSimpWin software and the calculated values are list in ESI† Table S2. From the calculated results, it can be seen that CNS@5%GR nanocomposite electrode has the lowest R_{ct} value (0.1749 $\Omega \cdot cm^{-2}$) and larger CPE (0.5093 mF). The charge-transfer resistance Rct, also called Faraday resistance, is a limiting factor for the specific power of the supercapacitor. It is the lower Faraday resistance that results in the high specific power of CNS@5%GR electrode. Thus, these EIS data reveal that the CNS@5%GR nanocomposite exhibit higher conductivity because of the presence of GR.

Conclusions

In summary, CoNi$_2$S$_4$/graphene nanocomposite with different loaded amount of graphene was obtained based on a facile physic approach. Due to the richer redox chemistry, higher electrochemical activity, higher electronic conductivity of CoNi$_2$S$_4$ nanoparticles and excellent electrical coupling to the underlying GR sheets, CNS@5%GR nanocomposite electrode presents an maximum high specific capacitance of 2099.1 F g^{-1} at a current density of 1 A g^{-1} and the specific capacitance can be maintained for 755.4 F g^{-1} at 4 A g^{-1} after 2000 charge–discharge cycles. Meantime, CNS@5%GR electrode shows excellent rate

capability (1046.4 F g^{-1} at 20 A g^{-1}) and better electrochemical reversibility. These results evidently suggest the great potential of the CoNi$_2$S$_4$/graphene nanocomposite electrode for high-performance SCs.

Notes and references

^{a} College of Chemistry and Chemical Engineering, Anyang Normal University, Anyang, Henan, 455002, China, Tel: +86-372-2900040; E-mail: duweimin75@gmail.com and huanpangchem@hotmail.com
^{b} College of Chemistry and Molecular Engineering, Zhengzhou University, Zhengzhou, Henan, 450001, China
^{c} School of Chemistry and Chemical Technology, Shanghai Jiao Tong University, Shanghai, 200240, China
† Electronic Supplementary Information (ESI) available: [The synthetic process of graphene; the electrochemical properties of CoNi$_2$S$_4$/graphene nanocomposite with different load of graphene (e.g.: 1%, 3%, 10%, 30%), CoNi$_2$S$_4$ nanoparticles, and graphene; Compared electrochemical performance between CoNi$_2$S$_4$/graphene nanocomposite and other nanomaterials; Calculated values of Rs, CPE, Rct, and Cp of the supercapacitor electrodes]. See DOI: 10.1039/b000000x/

1.   L. Dai, D. W. Chang, J.-B. Baek and W. Lu, *Small*, 2012, **8**, 1130-1166.
2.   S. L. Candelaria, Y. Shao, W. Zhou, X. Li, J. Xiao, J.-G. Zhang, Y. Wang, J. Liu, J. Li and G. Cao, *Nano Energy*, 2012, **1**, 195-220.
3.   C. Merlet, B. Rotenberg, P. A. Madden, P.-L. Taberna, P. Simon, Y. Gogotsi and M. Salanne, *Nat Mater*, 2012, **11**, 306-310.
4.   H. Sun, L. Cao and L. Lu, *Energ Environ Sci*, 2012, **5**, 6206.
5.   D. Sun, X. Yan, J. Lang and Q. Xue, *J Power Sources*, 2013, **222**, 52-58.
6.   A. L. M. Reddy, S. R. Gowda, M. M. Shaijumon and P. M. Ajayan, *Adv Mater*, 2012, **24**, 5045-5064.
7.   L. L. Zhang and X. S. Zhao, *Chem Soc Rev*, 2009, **38**, 2520.
8.   S. Bose, T. Kuila, A. K. Mishra, R. Rajasekar, N. H. Kim and J. H. Lee, *J Mater Chem*, 2012, **22**, 767.
9.   J. Yan, Z. J. Fan, W. Sun, G. Q. Ning, T. Wei, Q. Zhang, R. F. Zhang, L. J. Zhi and F. Wei, *Adv Funct Mater*, 2012, **22**, 2632-2641.
10.   Z.-S. Wu, G. Zhou, L.-C. Yin, W. Ren, F. Li and H.-M. Cheng, *Nano Energy*, 2012, **1**, 107-131.
11.   M. Zhi, C. Xiang, J. Li, M. Li and N. Wu, *Nanoscale*, 2013, **5**, 72.
12.   Q. Wang, L. Jiao, H. Du, J. Yang, Q. Huan, W. Peng, Y. Si, Y. Wang and H. Yuan, *Crystengcomm*, 2011, **13**, 6960-6963.
13.   C. Yuan, B. Gao, L. Su, L. Chen and X. Zhang, *J Electrochem Soc*, 2009, **156**, A199-A203.
14.   S. J. Bao, C. M. Li, C. X. Guo and Y. Qiao, *J Power Sources*, 2008, **180**, 676-681.
15.   F. Tao, Y. Q. Zhao, G. Q. Zhang and H. L. Li, *Electrochem Commun*, 2007, **9**, 1282-1287.
16.   T. Zhu, B. Xia, L. Zhou and X. Wen Lou, *J Mater Chem*, 2012, **22**, 7851-7855.
17.   L. Zhang, H. B. Wu and X. W. Lou, *Chem Commun*, 2012, **48**, 6912-6914.

18.   J. Y. Lin and S. W. Chou, *RSC Adv*, 2013, **3**, 2043-2048.
19.   C. Yuan, J. Li, L. Hou, X. Zhang, L. Shen and X. W. Lou, *Adv Funct Mater*, 2012, **22**, 4592-4597.
20.   G. Zhang and X. W. Lou, *Adv Mater*, 2013, **25**, 976-979.
21.   G. Q. Zhang, H. B. Wu, H. E. Hoster, M. B. Chan-Park and X. W. Lou, *Energ Environ Sci*, 2012, **5**, 9453-9456.
22.   C. Z. Yuan, J. Y. Li, L. R. Hou, L. Yang, L. F. Shen and X. G. Zhang, *J Mater Chem*, 2012, **22**, 16084-16090.
23.   F. L. Zhu, J. X. Zhao, Y. L. Cheng, H. B. Li and X. B. Yan, *Acta Phys-Chim Sin*, 2012, **28**, 2874-2878.
24.   H. B. Wu, H. Pang and X. W. Lou, *Energ Environ Sci*, 2013, **6**, 3619-3626.
25.   X. Wang, X. D. Han, M. Lim, N. Singh, C. L. Gan, M. Jan and P. S. Lee, *J Phys Chem C*, 2012, **116**, 12448-12454.
26.   D. Carriazo, J. Patino, M. C. Gutierrez, M. L. Ferrer and F. d. Monte, *RSC Adv*, 2013, **3**, 13690–13695.
27.   H. Chen, J. Jiang, L. Zhang, H. Wan, T. Qi and D. Xia, *Nanoscale*, 2013, **5**, 8879–8883.
28.   H. Wan, J. Jiang, J. Yu, K. Xu, L. Miao, L. Zhang, H. Chen and Y. Ruan, *Crystengcomm*, 2013, **15**, 7649–7651.
29.   S. Peng, L. Li, C. Li, H. Tan, R. Cai, H. Yu, S. Mhaisalkar, M. Srinivasan, S. Ramakrishna and Q. Yan, *Chem Commun*, 2013, **49**, 10178-10180.
30.   W. Du, Z. Zhu, Y. Wang, J. Liu, W. Yang, X. Qian and H. Pang, *RSC Adv*, 2014, **4**, 6998-7002.
31.   W. S. Hummers and R. E. Offeman, *J Am Chem Soc*, 1958, **80**, 1339-1339.
32.   P. Vitanov, A. Tsanev, P. Stefanov, A. Harizanova and T. Ivanova, *J Optoelectron Adv M*, 2007, **9**, 256-259.
33.   R. Zou, K. Xu, T. Wang, G. He, Q. Liu, X. Liu, Z. Zhang and J. Hu, *J Mater Chem A*, 2013, **1**, 8560-8566.
34.   Y. Ohno, *Phys Rev B*, 1991, **44**, 1281-1291.
35.   K. M. Abraham and S. M. Chaudhri, *J Electrochem Soc*, 1986, **133**, 1307-1311.
36.   A. B. Christie, J. Lee, I. Sutherland and J. M. Walls, *Appl Surf Sci*, 1983, **15**, 224-237.
37.   G. P. Wang, L. Zhang and J. J. Zhang, *Chem Soc Rev*, 2012, **41**, 797-828.
38.   G.-R. Li, Z.-L. Wang, F.-L. Zheng, Y.-N. Ou and Y.-X. Tong, *J Mater Chem*, 2011, **21**, 4217.
39.   Y. Q. Wu, X. Y. Chen, P. T. Ji and Q. Q. Zhou, *Electrochim Acta*, 2011, **56**, 7517-7522.
40.   J. Xu, X. F. Gu, J. Y. Cao, W. C. Wang and Z. D. Chen, *J Solid State Electr*, 2012, **16**, 2667-2674.
41.   Z. Tang, C. H. Tang and H. Gong, *Adv Funct Mater*, 2012, **22**, 1272-1278.
42.   Y. Hou, Y. Cheng, T. Hobson and J. Liu, *Nano Lett*, 2010, **10**, 2727-2733.